

# A new numerical method to construct binary neutron star initial data

**Wolfgang Tichy**

Department of Physics, Florida Atlantic University, Boca Raton, FL 33431, USA

**Abstract.**

We present a new numerical method for the generation of binary neutron star initial data using a method along the lines of the the Wilson-Mathews or the closely related conformal thin sandwich approach. Our method uses six different computational domains, which include spatial infinity. Each domain has its own coordinates which are chosen such that the star surfaces always coincide with domain boundaries. These properties facilitate the imposition of boundary conditions. Since all our fields are smooth inside each domain, we are able to use an efficient pseudospectral method to solve the elliptic equations associated with the conformal thin sandwich approach. Currently we have implemented corotating configurations with arbitrary mass ratios, but an extension to arbitrary spins is possible. The main purpose of this paper is to introduce our new method and to test our code for several different configurations.

PACS numbers: 04.25.dk, 04.30.Db, 97.60.Jd, 97.80.Fk

## 1. Introduction

Currently several gravitational wave detectors such as LIGO [1, 2], Virgo [3, 4] or GEO [5] are already operating, while several others are in the planning or construction phase [6]. One of the most promising sources for these detectors are the inspirals and mergers of binary neutron stars (NS). In order to make predictions about the final phase of such inspirals and mergers, fully non-linear numerical simulations of the Einstein Equations are required. To start such simulations initial data are needed. The emission of gravitational waves tends to circularize the orbits [7, 8]. Thus, during the inspiral, we expect the two NSs to be in quasicircular orbits around each other with a radius which shrinks on a timescale much larger than the orbital timescale. This means that the initial data should have an approximate helical Killing vector  $\xi^\mu$ . In addition, one would like to have the initial data in coordinates such that this approximate symmetry is manifest, i.e. the time evolution vector should lie along  $\xi^\mu$ , so that the time derivatives of the evolved quantities are minimized. In order to achieve these goals we use the Wilson-Mathews approach [9, 10], which is closely related to the conformal thin sandwich formalism [11]. The Wilson-Mathews approach approach has already been successfully used by several groups. Among them are results for corotating [12, 13, 14, 15] and irrotational [16, 17, 18, 19, 20] NS binaries with equal masses. One group has also produced results for unequal mass systems [21, 22].

In this paper we present a new numerical method to construct initial data for binary NSs in corotating configurations for arbitrary mass ratios. The main focus is on the numerical method rather than on new physics. We describe an efficient implementation of this method with the SGRID code [23], discuss code tests, and compare with previous results.

Throughout we will use units where  $G = c = 1$ . Later when we present numerical results we will use fully dimensionless units by setting  $\kappa$  in the polytropic equation of state to  $\kappa = G = c = 1$ . Latin indices such as  $i$  run from 1 to 3, while Greek indices such as  $\mu$  run from 0 to 3. The paper is organized as follows. In Sec. 2 we describe the General Relativistic equations that govern binary neutron stars described by perfect fluids. Sec. 3 describes our particular numerical implementation of these equations, followed by results for some particular configurations in Sec. 4. We conclude with a discussion of our method in Sec. 5.

## 2. Binary neutron stars in General Relativity

In this section we describe the equations governing binary NSs in quasi circular orbits.

### 2.1. ADM decomposition of Einstein's equations

We use the Arnowitt-Deser-Misner (ADM) decomposition of Einstein's equations (see e.g. [24]) and write the line element

$$ds^2 = -\alpha^2 dt^2 + \gamma_{ij}(dx^i + \beta^i)(dx^j + \beta^j) \quad (1)$$

in terms of the lapse  $\alpha$ , shift  $\beta^i$  and the 3-metric  $\gamma_{ij}$ . The extrinsic curvature is defined by

$$K_{ij} = -\frac{1}{2\alpha}(\partial_t \gamma_{ij} - \mathcal{L}_\beta \gamma_{ij}), \quad (2)$$

With these definitions Einstein's equations split into the evolution equations

$$\begin{aligned} \partial_t \gamma_{ij} &= -2\alpha K_{ij} + \mathcal{L}_\beta \gamma_{ij} \\ \partial_t K_{ij} &= \alpha(R_{ij} - 2K_{il}K_j^l + KK_{ij}) - D_i D_j \alpha + \mathcal{L}_\beta K_{ij} \\ &\quad - 8\pi S_{ij} + 4\pi \gamma_{ij}(S - \rho) \end{aligned} \quad (3)$$

and the Hamiltonian and momentum constraint equations

$$\begin{aligned} R - K_{ij}K^{ij} + K^2 &= 16\pi\rho \\ D_j(K^{ij} - \gamma^{ij}K) &= 8\pi j^i. \end{aligned} \quad (4)$$

Here  $R_{ij}$  and  $R$  are the Ricci tensor and scalar computed from  $\gamma_{ij}$ ,  $D_i$  is the derivative operator compatible with  $\gamma_{ij}$  and all indices here are raised and lowered with the 3-metric  $\gamma_{ij}$ . The source terms  $\rho$ ,  $j^i$ ,  $S_{ij}$  and  $S = \gamma^{ij}S_{ij}$  are projections of the stress-energy tensor  $T_{\mu\nu}$  given by

$$\begin{aligned} \rho &= T_{\mu\nu}n^\mu n^\nu \\ j^i &= -T_{\mu\nu}n^\mu \gamma^{\nu i} \\ S^{ij} &= T_{\mu\nu}\gamma^{\mu i}\gamma^{\nu j} \end{aligned} \quad (5)$$

and correspond to the energy density, flux and stress-tensor. The vector  $n^\mu$  appearing here is the the 4-vector normal to a  $t = \text{const}$  slice.

## 2.2. Decomposition of 3-metric and extrinsic curvature

As in [9, 10] the 3-metric  $\gamma_{ij}$  is decomposed into a conformal factor  $\psi$  and a conformal metric  $\bar{\gamma}_{ij}$  such that

$$\gamma_{ij} = \psi^4 \bar{\gamma}_{ij}. \quad (6)$$

The extrinsic curvature is split into its trace  $K$  and its tracefree part  $A_{ij}$  by writing it as

$$K_{ij} = A_{ij} + \frac{1}{3}\gamma_{ij}K \quad (7)$$

## 2.3. Quasi equilibrium assumptions

We now make some additional simplifying assumptions. First we assume that our binary is in an approximately circular orbit and that the stars are corotating. This implies the existence of an approximate helical Killing vector  $\xi^\mu$ . In a coordinate system where this helical symmetry is manifest and the time evolution vector lies along  $\xi^\mu$ , all time derivatives should approximately be zero. Here we only assume that the time derivative  $\partial_t \bar{\gamma}_{ij}$  of the conformal metric and the time derivative  $\partial_t K$  of the trace of the extrinsic

curvature vanish. The former allows us to express the extrinsic curvature in terms of the shift and results in

$$A^{ij} = \frac{1}{2\psi^4\alpha}(\bar{L}\beta)^{ij}, \quad (8)$$

where

$$(\bar{L}\beta)^{ij} = \bar{D}^i\beta^j + \bar{D}^j\beta^i - \frac{2}{3}\bar{D}_k\beta^k, \quad (9)$$

and  $\bar{D}_k$  is the derivative operator compatible with  $\bar{\gamma}_{ij}$ . The assumption  $\partial_t K = 0$  together with the evolution equation of  $K$  (derived from Eq. (3)) implies

$$\begin{aligned} \psi^{-5}[\bar{D}_k\bar{D}^k(\alpha\psi) - \alpha\bar{D}_k\bar{D}^k\psi] &= \alpha(R + K)^2 + \beta^i\bar{D}_iK \\ &+ 4\pi\alpha(S - 3\rho). \end{aligned} \quad (10)$$

#### 2.4. Further simplifications and boundary conditions

Next we also choose a maximal slice and thus  $K = 0$ , and assume that the conformal 3-metric is flat and given by [9, 10]

$$\bar{\gamma}_{ij} = \delta_{ij}. \quad (11)$$

This latter assumption merely simplifies our equations and could in principle be improved by e.g. choosing a post-Newtonian expression for  $\bar{\gamma}_{ij}$  as in [25, 26]. Using Eq. (11) the Hamiltonian and momentum constraints in Eq. (4) and Eq. (10) simplify and we obtain

$$\begin{aligned} \bar{D}^2\psi &= -\frac{\psi^5}{32\alpha^2}(\bar{L}B)^{ij}(\bar{L}B)_{ij} - 2\pi\psi^5\rho \\ \bar{D}_j(\bar{L}B)^{ij} &= (\bar{L}B)^{ij}\bar{D}_j\ln(\alpha\psi^{-6}) + 16\pi\alpha\psi^4j^i \\ \bar{D}^2(\alpha\psi) &= \alpha\psi\left[\frac{7\psi^4}{32\alpha^2}(\bar{L}B)^{ij}(\bar{L}B)_{ij} + 2\pi\psi^4(\rho + 2S)\right], \end{aligned} \quad (12)$$

where  $(\bar{L}B)^{ij} = \bar{D}^iB^j + \bar{D}^jB^i - \frac{2}{3}\delta^{ij}\bar{D}_k B^k$ ,  $\bar{D}_i = \partial_i$ , and

$$B^i = \beta^i + \omega\epsilon^{ij3}(x^j - x_{CM}^j). \quad (13)$$

Here  $x_{CM}^i$  denotes the center of mass position and  $\omega$  is the orbital angular velocity, which we have chosen to lie along the  $z$ -direction. The elliptic equations (12) have to be solved subject to the boundary conditions

$$\lim_{r\rightarrow\infty}\psi = 1, \quad \lim_{r\rightarrow\infty}B^i = 0, \quad \lim_{r\rightarrow\infty}\alpha\psi = 1. \quad (14)$$

at spatial infinity.

### 2.5. Matter equations

We assume that the matter in both stars is a perfect fluid with a stress-energy tensor

$$T^{\mu\nu} = [\rho_0(1 + \epsilon) + P]u^\mu u^\nu + P g^{\mu\nu}. \quad (15)$$

Here  $\rho_0$  is the mass density (which is proportional the number density of baryons),  $P$  is the pressure,  $\epsilon$  is the internal energy density divided by  $\rho_0$ ,  $u^\mu$  is the 4-velocity of the fluid and  $g^{\mu\nu}$  is the spacetime metric. The matter variables in Eq.(5) are then

$$\begin{aligned} \rho &= \alpha^2[\rho_0(1 + \epsilon) + P]u^0 u^0 - P \\ j^i &= \alpha[\rho_0(1 + \epsilon) + P]u^0 u^0 (u^i/u^0 + \beta^i) \\ S^{ij} &= [\rho_0(1 + \epsilon) + P]u^0 u^0 (u^i/u^0 + \beta^i)(u^j/u^0 + \beta^j) \\ &\quad + P\gamma^{ij} \end{aligned} \quad (16)$$

The fact that  $\nabla_\nu T^{\mu\nu} = 0$  yields the relativistic Euler equation

$$[\rho_0(1 + \epsilon) + P]u^\nu \nabla_\nu u^\mu = -(g^{\mu\nu} + u^\mu u^\nu)\nabla_\nu P, \quad (17)$$

which together with the continuity equation

$$\nabla_\nu(\rho_0 u^\nu) = 0 \quad (18)$$

governs the fluid.

For corotating stars we can show that the continuity equation (18) is identically satisfied. Furthermore one can show that the Euler equation leads to (see e.g. problem 16.17 in [27])

$$[\rho_0(1 + \epsilon) + P]d \ln(u_\mu \xi^\mu) = -dP, \quad (19)$$

where  $\xi^\mu$  is the assumed helical Killing vector. With the help of the first law of thermodynamics ( $d[\rho_0(1 + \epsilon)] = [\rho_0(1 + \epsilon) + P]d\rho_0/\rho_0$ ) this equation can be integrated to yield

$$u_\mu \xi^\mu = \frac{C_{1/2} \rho_0}{\rho_0(1 + \epsilon) + P}, \quad (20)$$

where  $C_{1/2}$  are constants of integration for each star. We will later choose them such that the rest mass of each star has a prescribed value. In corotating coordinates and taking into account our conformally flat 3-metric,  $u_\mu \xi^\mu$  can be written as

$$u_\mu \xi^\mu = -1/u^0 = -[\alpha^2 - \psi^4 \delta_{ij} \beta^i \beta^j]^{1/2}. \quad (21)$$

In order simplify the problem we assume a polytropic equation of state

$$P = \kappa \rho_0^{1+1/n}. \quad (22)$$

It is then convenient to introduce the dimensionless ratio

$$q = P/\rho_0, \quad (23)$$

which we use to write

$$\begin{aligned} \rho_0 &= \kappa^{-n} q^n \\ P &= \kappa^{-n} q^{n+1} \\ \epsilon &= nq. \end{aligned} \quad (24)$$

### 3. Numerical method

In order to construct binary NS initial data we have to solve the five elliptic equations in Eq. (12), with the matter terms given by Eqs. (16), (21) and (24). In addition, our data also have to satisfy Eq. (20), which can be expressed as

$$q = \frac{1}{n+1} \left( \frac{C_{1/2}}{u_\mu \xi^\mu} - 1 \right) \quad (25)$$

for each star. We will solve the whole set of equations by iterating over the following steps: (i) We first come up with an initial guess for  $q$  in each star, in practice we simply choose Tolman-Oppenheimer-Volkoff (TOV) solutions (see e.g. Chap. 23 in [24]) for each. (ii) Next we solve the 5 coupled elliptic equations (12) for this given  $q$ . (iii) Then we use Eq. (25) to update  $q$  in each star. The constants  $C_{1/2}$  in general have different values for each star. We adjust the value for each star such that it has a prescribed rest mass. After updating  $q$  we go back to step (ii) and iterate until all equations are satisfied up to a given tolerance.

#### 3.1. Coordinates adapted to star surfaces

Note that the matter is smooth inside the stars. However, at the surface (at  $q = 0$ ),  $\rho_0$ ,  $P$  and  $\epsilon$  are not differentiable. This means that if we want to take advantage of a spectral method, the star surfaces should be domain boundaries. A difficulty with our iterative approach, however, is that each time we update  $q$  the matter distributions change, so that the stars change shape or even move. Hence the domain boundaries have to be changed as well. In order to address this problem we introduce several domains each with its own coordinates. These coordinates depend on two freely specifiable functions which will allow us to vary the location of the domain boundaries, so that we can always adapt our domains to the current star surfaces in each iteration. As in the initial data approaches in [28, 29] our aim was to introduce as few domains as possible.

The coordinates we will use, are very similar to the ones introduced by Ansorg [30]. We place both stars on the  $x$ -axis and write down the necessary coordinate transformations in two steps. First we express the standard Cartesian coordinates as

$$\begin{aligned} x &= \frac{b}{2} \left[ \frac{1}{(X^2 + R^2)^2} + 1 \right] (X^2 - R^2) \\ y &= b \left[ \frac{1}{(X^2 + R^2)^2} - 1 \right] X R \cos \phi \\ z &= b \left[ \frac{1}{(X^2 + R^2)^2} - 1 \right] X R \sin \phi, \end{aligned} \quad (26)$$

where  $b$  is a parameter related to the distance between the stars, and  $X, R$  are functions of the new coordinates  $(A, B, \phi)$  we will use in each domain. Note that spatial infinity is located at the point where  $X = R = 0$  and that in order to cover all  $(x, y, z)$  it is sufficient to restrict  $X, R, \phi$  to the ranges  $0 \leq X \leq 1$ ,  $0 \leq R \leq \sqrt{1 - X^2}$  and  $0 \leq \phi \leq 2\pi$ . In order to complete the coordinate transformation between the Cartesian

$(x, y, z)$  and the new coordinates  $(A, B, \phi)$ , we now write down  $X$  and  $R$  as functions of  $(A, B, \phi)$ . Inside star1 we use

$$\begin{aligned} X &= (1 - A)\{\Re[C_+(B, \phi)] - B\Re[C_+(1, \phi)]\} \\ &\quad + B \cos([1 - A] \arg[C_+(1, \phi)]) + (1 - B)A \\ R &= (1 - A)\{\Im[C_+(B, \phi)] - B\Im[C_+(1, \phi)]\} \\ &\quad + B \sin([1 - A] \arg[C_+(1, \phi)]), \end{aligned} \tag{27}$$

where the strictly positive function  $\sigma_+(B, \phi)$  in

$$C_+(B, \phi) = \sqrt{\tanh\left(\frac{\sigma_+(B, \phi) + i\pi B}{4}\right)} \tag{28}$$

determines the shape of the star surface. The surface is always located at  $A = 0$  but depending on the choice for  $\sigma_+(B, \phi)$  it will be at different  $(x, y, z)$ , e.g. for  $\sigma_+(B, \phi) = \text{const}$  we will get a spherical surface in  $(x, y, z)$ . Note that this star is located around  $x = b$ . Inside star2 we use a similar transformation given by

$$\begin{aligned} X &= (1 - A)\{\Re[C_-(B, \phi)] - B\Re[C_-(1, \phi)]\} \\ &\quad + B \cos\left(\frac{\pi}{2}A + [1 - A] \arg[C_-(1, \phi)]\right) \\ R &= (1 - A)\{\Im[C_-(B, \phi)] - B\Im[C_-(1, \phi)]\} \\ &\quad + B \sin\left(\frac{\pi}{2}A + [1 - A] \arg[C_-(1, \phi)]\right) + (1 - B)A, \end{aligned} \tag{29}$$

where the strictly negative function  $\sigma_-(B, \phi)$  in

$$C_-(B, \phi) = \sqrt{\tanh\left(\frac{\sigma_-(B, \phi) + i\pi B}{4}\right)} \tag{30}$$

determines where the star surface ( $A = 0$ ) is located in  $(x, y, z)$  coordinates. Star2 is located around  $x = -b$ . Note that the  $A, B, \phi$  coordinates are different inside each star, but in order to cover each star their ranges are  $0 \leq A \leq 1$ ,  $0 \leq B \leq 1$  and  $0 \leq \phi \leq 2\pi$  in each case.

The outside of both stars is covered by two additional domains. The first one covers the region outside star1 for all positive  $x$ , while the second one covers the region outside star2 for all negative  $x$ . Both coordinate transformations can be written as

$$\begin{aligned} X &= (1 - A)\{\Re[C_\pm(B, \phi)] - B\Re[C_\pm(1, \phi)]\} \\ &\quad + B \cos\left(\frac{\pi}{4}A + [1 - A] \arg[C_\pm(1, \phi)]\right) \\ R &= (1 - A)\{\Im[C_\pm(B, \phi)] - B\Im[C_\pm(1, \phi)]\} \\ &\quad + B \sin\left(\frac{\pi}{4}A + [1 - A] \arg[C_\pm(1, \phi)]\right), \end{aligned} \tag{31}$$

where we use  $C_+(B, \phi)$  in the former and  $C_-(B, \phi)$  in the latter. In each case the star surface is at  $A = 0$  and spatial infinity is at  $(A, B) = (1, 0)$ .

Figure 1 shows the coordinate lines in  $z = 0$  plane.

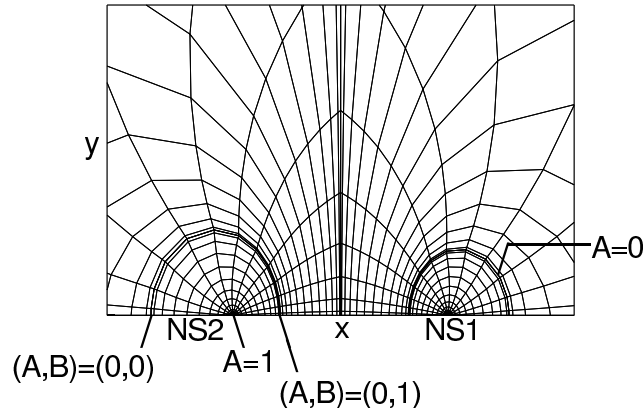


**Figure 1.** The plot shows the lines of constant  $A$  and  $B$  in the  $xy$ -plane for  $b = 1.84$ ,  $\sigma_+(B, \phi) = 1.51$  and  $\sigma_-(B, \phi) = -1.28$ . The two neutron stars are marked with NS1 and NS2. In addition, the  $(x, y)$  positions of a few points are indicated. The coordinate singularities at  $A = 1$  inside the stars are located at  $x = \pm b$ .

### 3.2. Spectral method

In order to solve the elliptic equations (12) we use the SGRID code [23] which employs pseudospectral methods to accurately compute spatial derivatives. We use Chebyshev expansions in the  $A$ - and  $B$ -directions and Fourier expansions  $\phi$ -direction. As collocation points we choose

$$\begin{aligned} A_l &= \frac{1}{2} \left[ 1 - \cos \left( \frac{\pi l}{n_A - 1} \right) \right] \\ B_j &= \frac{1}{2} \left[ 1 - \cos \left( \frac{\pi j}{n_B - 1} \right) \right] \\ \phi_k &= \frac{2\pi k}{n_\phi}, \end{aligned} \quad (32)$$

where  $l, j, k$  are integers obeying

$$0 \leq l < n_A, \quad 0 \leq j < n_B, \quad 0 \leq k < n_\phi. \quad (33)$$

The number  $n_A$ ,  $n_B$  and  $n_\phi$  of collocation points in each direction is chosen to be equal in all four domains, to ensure that the grid points on the boundaries of two adjacent domains will be at the same  $(x, y, z)$  location. As in [23] we will solve Eq. (12) as written down in Cartesian form and compute derivatives like  $\partial_x \psi$  using the chain rule:

$$\partial_x \psi = \frac{\partial A}{\partial x} \partial_A \psi + \frac{\partial B}{\partial x} \partial_B \psi + \frac{\partial \phi}{\partial x} \partial_\phi \psi. \quad (34)$$

Note that all points with  $B = 0$  or  $B = 1$  lie along the  $x$ -axis, with  $x$  independent of  $\phi$ . Hence along this axis we have the standard coordinate singularity of polar coordinates. Furthermore, all points with  $A = 1$  in the interior of each star correspond to just one point on the  $x$ -axis. Thus there is an additional coordinate singularity at  $A = 1$  inside each star. We have found that if we simply use the  $A, B, \phi$  coordinates as described above we were not able to solve the elliptic equations (12). The culprit is the singularity at  $A = 1$  inside each star. Near these points the Jacobian

matrix  $\frac{\partial(A,B,\phi)}{\partial(x,y,z)}$  blows up so strongly that we cannot accurately compute derivatives using Eq. (34). This problem would also occur if we did use the exact same coordinates as proposed by Ansorg [30]. In [30] the problem is not addressed since for black holes one can use excision boundary conditions and does not need the inner domains. One way around this problem would be to construct different basis functions, which would have to be chosen such that they have vanishing  $B$  and  $\phi$  derivatives at  $A = 1$ . However, then we would not be able to use Fast Fourier transforms anymore to compute derivatives. For this reason we have chosen a different approach. We simply restrict the range of  $A$  inside each star so that inside  $0 \leq A \leq A_{max} < 1$ . The collocation points in  $A$  inside the stars are then given by

$$A_l = \frac{A_{max}}{2} \left[ 1 - \cos \left( \frac{l\pi}{n_A - 1} \right) \right]. \quad (35)$$

We typically choose  $A_{max} = 0.85$ . In this way we completely avoid the singularities at  $A = 1$ . Of course then, our inner domains do not cover the entire star interiors any more. Instead they leave out a small hole around  $A = 1$ . We simply cover this hole by placing two additional cubical domains inside each star. Each cube is chosen such that completely covers the hole (described by  $A_{max} < A \leq 1$ ). In each cube we use standard Cartesian coordinates so that it overlaps with part of the inner domain covered by the  $A, B, \phi$  coordinates. The collocation points inside each cube are then

$$\begin{aligned} x_l &= \frac{x_{min} - x_{max}}{2} \cos \left( \frac{l\pi}{n_c - 1} \right) + \frac{x_{min} + x_{max}}{2} \\ y_j &= \frac{y_{min} - y_{max}}{2} \cos \left( \frac{j\pi}{n_c - 1} \right) + \frac{y_{min} + y_{max}}{2} \\ z_k &= \frac{z_{min} - z_{max}}{2} \cos \left( \frac{k\pi}{n_c - 1} \right) + \frac{z_{min} + z_{max}}{2}, \end{aligned} \quad (36)$$

where the minima and maxima  $x_{min}, x_{max}, y_{min}, y_{max}, z_{min}, z_{max}$  are chosen such that the cube covers the hole, and where  $n_c = 6$  is typically sufficient, since the cubes are very small. Figure 2 shows how a cube is fitted into star1.

In order to numerically solve the elliptic equations in Eq. (12) we arrange the values of the fields  $\psi, B^i$  and  $\alpha\psi$  at each grid point in a vector  $w$ . Since we solve for 5 fields, the dimension of this vector is five times the total number of grid points. In order to find a  $w$  that satisfies Eq. (12) we impose Eq. (12) at all interior grid points. At adjacent domain boundaries we impose the conditions that fields and their normal derivatives are equal on both sides. At infinity we impose Eq. (14). In the domains covered by the  $A, B, \phi$  coordinates we impose the following regularity conditions along the  $x$ -axis: For  $k > 0$  we demand

$$\Psi(A_l, B_j, \phi_k) = \Psi(A_l, B_j, \phi_0), \quad (37)$$

while for  $k = 0$  we impose

$$\partial_s \Psi(A_l, B_j, \phi_0) + \partial_s \partial_\phi \partial_\phi \Psi(A_l, B_j, \phi_0) = 0. \quad (38)$$

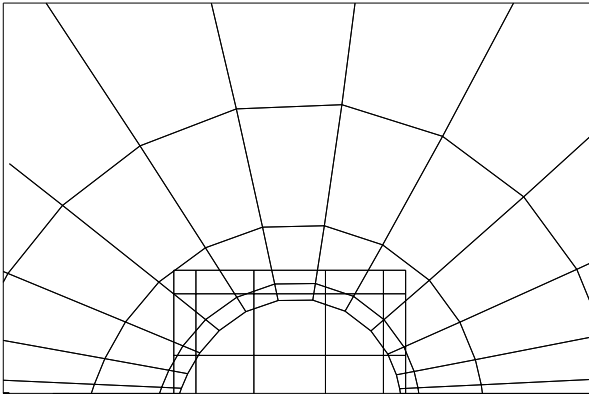


**Figure 2.** In order to avoid the coordinate singularity at  $A = 1$  inside the stars, we have restricted the range of  $A$  to  $0 \leq A \leq 0.85$ . The remaining space is filled with a small cube of length  $0.016b$ . This figure is a blowup of the inside of NS1 in Fig. 1 where the small cubes are not visible.

Here  $\Psi$  stands for either  $\psi$ ,  $B^i$  or  $\alpha\psi$ , and  $s = \sqrt{y^2 + z^2}$  is the distance from the  $x$ -axis. In order to deal with the cubes which overlap the  $A, B, \phi$  covered domains inside each star, we impose the condition that the fields at points on the cube boundaries must be equal to the fields in the  $A, B, \phi$  covered domain interpolated to these points. Correspondingly we also demand that the fields at points on the  $A = A_{max}$  boundaries must equal to the fields in the cube interpolated to these points. This interpolation is done with our given spectral accuracy. To compute a field at a point that is not a collocation point, we first compute the spectral expansion coefficients from the field values at the collocation points in the domain of interest. To interpolate to any point in this domain we then compute the field value from a sum over coefficients times the basis functions evaluated at the point in question. This last interpolation step can be computationally expensive if we interpolate onto many points, while going between field values and collocation points can be done via Fast Fourier transforms and is thus not very expensive. Note, however, that in our case these interpolations are not too costly, because our cubical domains have only  $6^3$  grid points. Such a small number of points should always be sufficient because the cubic domains are so small so that all fields are nearly constant inside the cubes, e.g. on the scale of Fig. 1 the cubes are not visible. This is an advantage over the domain decomposition used in [31, 17] where interpolations are needed between domains with many more grid points.

If we take all these conditions into account we obtain  $N = 4n_A n_B n_\phi + 2n_c^3$  non-linear equations of the form

$$f_m(w) = 0, \quad m = 1, 2, \dots, N \quad (39)$$

for the  $N$  unknowns comprising the solution vector  $w$ . We solve this system of equations by a Newton-Raphson scheme. This scheme requires an initial guess, for which we simply use two TOV solutions in conformally flat isotropic coordinates. In order to solve the

linearized equations

$$\frac{\partial f_m(w)}{\partial w^n} x^n = -f_m(w) \quad (40)$$

in each Newton-Raphson step, we note that  $f_m(w)$  contains spectral derivatives of  $w$  in different directions, so that the  $N \times N$  matrix  $\frac{\partial f_m(w)}{\partial w^n}$  is sparse in the sense that it contains about 95% zeros. So in order to numerically solve the linearized Eq. (40) we use the sparse matrix solver UMFPACK [32, 33, 34, 35, 36].

### 3.3. Iteration scheme

As already mentioned solving the elliptic equations in Eq. (12) once is not enough. After each solve, we have to adjust  $q$  using Eq. (25). This adjustment presents the problem that the star surfaces (located at  $q = 0$ ) change. Hence we have to also adjust  $\sigma_+(B, \phi)$  and  $\sigma_-(B, \phi)$  in order to keep both star surfaces at  $A = 0$ . While this adjustment is not hard to implement, it incurs a high computational cost since adjusting  $\sigma_+(B, \phi)$  and  $\sigma_-(B, \phi)$  amounts to changing our computational grid, and after each such adjustment we need to interpolate all relevant fields onto the new grid. In addition, the adjustment has to be carried out several times after each individual elliptic solve, since we were only able to achieve a stable iteration scheme if we pick the free constants  $C_1$ ,  $C_2$ ,  $\omega$  and  $x_{CM}$  as follows. Let us call the intersection points of the  $x$ -axis with the side of the star surface not facing the origin  $x_{out1}$  and  $x_{out2}$  (located at  $(A, B) = (0, 0)$ ) for each star. We then determine  $\omega$  and  $x_{CM}$  by requiring that  $x_{out1}$  and  $x_{out2}$  remain constant. This task is accomplished by a root finder. In each iteration of this root finder  $C_1$ ,  $C_2$  are adjusted such that the rest mass of each star remains constant (by another root finder). These root finders have to evaluate  $q$  and thus need to adjust the domain shapes several times. If we do not adjust  $\omega$  and  $x_{CM}$  we find that the stars drift around too much for the iterations to converge. Instead of  $x_{out1}$  and  $x_{out2}$  it is also possible to fix the points  $x_{max1}$  and  $x_{max2}$  where the maximum values of  $q$  occur.

In addition, we have observed that once a new  $q$  is set the elliptic solve often "overcorrects" which again can result in an unstable iteration scheme. To overcome this problem we typically do not take the  $\psi$ ,  $B^i$  and  $\alpha\psi$  coming from solving Eq. (12) as our new fields. Rather, we take the average of this solution and the  $\psi$ ,  $B^i$  and  $\alpha\psi$  from the previous iteration step as our new fields. In this way  $\psi$ ,  $B^i$  and  $\alpha\psi$  change less from one iteration step to the next.

## 4. Results

All the results presented in this section were computed for  $n = 1$  polytopes (see Eq. (22)) in units where  $\kappa = 1$ .

In order to check that our SGRID code is working properly we have checked the convergence of the constraints. For these tests we have computed the constraints directly from Eq. (4) for different numbers of grid points. From Fig. 3 we see that

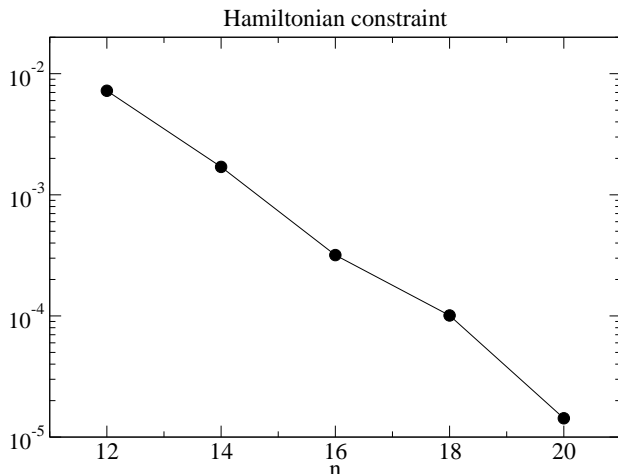


**Figure 3.** The  $L^2$ -norm of the Hamiltonian constraint on the grid inside star 1 converges exponentially with the number of grid points  $n_A = n_B = n$ . The plot is for an equal mass binary with rest masses  $m_{01} = m_{02} = 0.05952$ . The star centers are located at  $x_{max1} = -x_{max2} = 2.112$ , and  $n_\phi = 8$  and  $n_c = 6$  are kept fixed.

the Hamiltonian constraint converges exponentially with the number of grid points, as expected for a spectral method. The momentum constraints as well as  $\partial_t K$  converge to zero in a similar fashion.

We have computed initial data for the configurations listed in table 1. Each configuration is described by the rest masses  $m_{01}$  and  $m_{02}$  of the two stars given by

$$m_{0i} = \int_{\text{star}_i} \rho_0 u^0 \alpha \psi^6 d^3x, \quad i = \{1, 2\} \quad (41)$$

and the separation parameter  $b$ , which appears in the coordinate transformations and is approximately half the separation. For each configuration we have also computed the ADM mass and angular momentum given by

$$M_{ADM} = \int \left( \rho + \frac{1}{64\pi\alpha^2} (\bar{L}B)^{ij} (\bar{L}B)_{ij} \right) \psi^5 d^3x \quad (42)$$

and

$$J_{ADM} = \int [(x - x_{CM})j^y - yj^x] \psi^{10} d^3x. \quad (43)$$

Our iterative scheme also yields the orbital angular velocity  $\omega$  and the location of the center of mass  $x_{CM}$ . Furthermore we list the maximum values of  $q$  in each star along the  $x$ -axis, together with their  $x$ -coordinates, and also the locations of the inner and outer edges of each star. We also show the distance  $d_{12}$  between the stars and star diameters  $d_{1/2}$  defined by  $d_{12} = |x_{max1} - x_{max2}|$  and  $d_{1/2} = |x_{out1/2} - x_{in1/2}|$ . The equal mass configuration in table 1 is very close to configurations already computed by Baumgarte et al. [13] and also by Gourgoulhon et al. [17] and agrees with those to better than 1% (see Table II. in [17]). Note that our code has no problems handling unequal mass systems, as well as systems that are far apart. In addition, it is very memory efficient. A typical run with  $n_A = n_B = 18$  points needs only about 80MB of memory. The initial data can thus be generated on ordinary PCs. On a 2.3GHz Linux PC it takes about 30

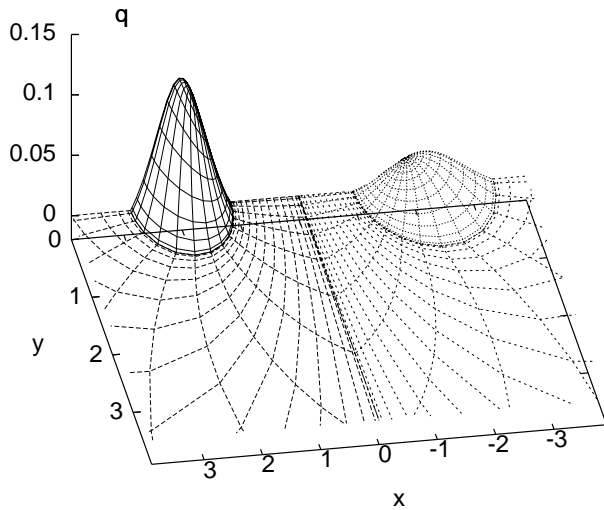
|  |         |         |        |        |
|--|---------|---------|--------|--------|
| $m_{01}$   | 0.05952 | 0.1400  | 0.140  | 0.150  |
| $m_{02}$   | 0.05952 | 0.0600  | 0.100  | 0.050  |
| $b$  | 1.8412  | 1.8400  | 10.00  | 5.00   |
| $M_{ADM}$  | 0.11572 | 0.18871 | 0.2263 | 0.1881 |
| $J_{ADM}$  | 0.02315 | 0.04233 | 0.122  | 0.0527 |
| $\omega$   | 0.038   | 0.048   | 0.0052 | 0.013  |
| $d_{12}$   | 4.224   | 4.174   | 20.09  | 10.20  |
| $d_1$  | 2.276   | 1.711   | 1.70   | 1.63   |
| $d_2$  | 2.276   | 2.398   | 1.96   | 2.25   |
| $x_{CM}$   | 0       | 0.74    | 1.6    | 2.4    |
| $q_{max1}$   | 0.0285  | 0.106   | 0.108  | 0.127  |
| $q_{max2}$   | 0.0285  | 0.0282  | 0.0588 | 0.0235 |
| $x_{in1}$  | +0.975  | +1.174  | +9.19  | +4.25  |
| $x_{max1}$   | +2.112  | +2.029  | +10.04 | +5.07  |
| $x_{out1}$   | +3.251  | +2.885  | +10.89 | +5.88  |
| $x_{in2}$  | -0.975  | -0.927  | -9.07  | -4.00  |
| $x_{max2}$   | -2.112  | -2.145  | -10.05 | -5.13  |
| $x_{out2}$   | -3.251  | -3.325  | -11.03 | -6.25  |
| $\frac{M_{ADM}}{M_{\odot}} \left(\frac{\kappa_0}{\kappa}\right)^{n/2}$ | 1.7524  | 2.8578  | 3.427  | 2.849  |
| $m_{01}/M_{ADM}$   | 0.5143  | 0.7419  | 0.619  | 0.797  |
| $m_{02}/M_{ADM}$   | 0.5143  | 0.3179  | 0.442  | 0.266  |
| $d_{12}/M_{ADM}$   | 36.50   | 22.12   | 88.78  | 54.23  |
| $d_1/M_{ADM}$  | 19.67   | 9.067   | 7.51   | 8.67   |
| $d_2/M_{ADM}$  | 19.67   | 12.71   | 8.66   | 12.0   |
| $\omega M_{ADM}$   | 0.0044  | 0.0091  | 0.0012 | 0.0024 |
| $J_{ADM}/M_{ADM}^2$  | 1.729   | 1.189   | 2.382  | 1.489  |

**Table 1.** Properties of initial data for different parameters  $m_{01}$ ,  $m_{02}$  and  $b$ . The numbers are first given in units of  $G = c = \kappa = 1$ . The total ADM mass  $M_{ADM}$  is also given in solar masses where  $\kappa_0 = 5 \times 10^8 \text{m}^2$  and  $n = 1$  (Note that  $\kappa^{-n/2} GM_{ADM}/c^2$  is dimensionless). After that we also list some quantities in geometric units ( $G = c = 1$ ) in terms of the total ADM mass.

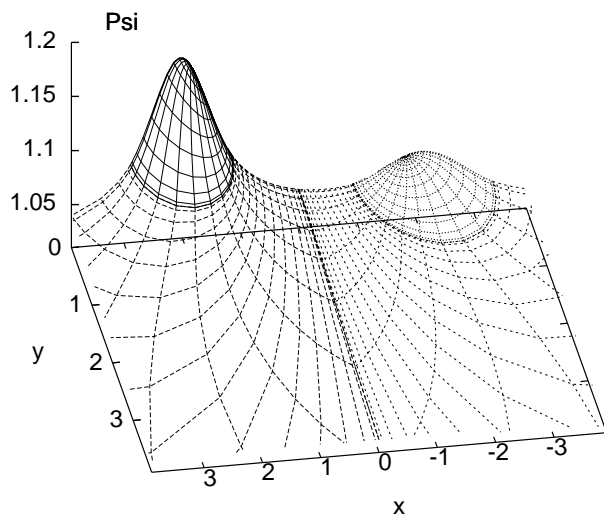
hours to push the Hamiltonian constraint down to  $10^{-4}$  if we use  $n_A = n_B = 18$  points. The main reason for the low memory footprint is that our spectral code needs only very few grid points to achieve the quoted accuracies.

Figure 4 shows  $q$  in the  $xy$ -plane for a binary with rest masses  $m_{01} = 0.14$  and  $m_{02} = 0.06$ . We can see how the domain boundaries are adapted such that  $q$  is non-zero only in the inner domains. Note that  $q$  is the rest mass density for  $\kappa = n = 1$ . In Figs. 5 and 6 we show the conformal factor  $\psi$  and the largest shift component  $B_y$  for the same configuration. Note that unlike  $q$  both are smooth ( $C^1$ ) across the domain boundaries.

In order to further verify our code we have performed a comparison with previous results from Taniguchi et al. [21]. In Figs. 7 and 8 we show how  $M_{ADM}$  and  $J_{ADM}$  vary as a function of  $\omega$  for a binary with rest masses  $m_{01} = 0.1461$  and  $m_{02} = 0.1299$ . As we can see our results (squares) approach the expected post-Newtonian results (taken



**Figure 4.**  $q$  in the  $xy$ -plane for a binary with rest masses  $m_{01} = 0.14$ ,  $m_{02} = 0.06$  and  $b = 1.84$ .



**Figure 5.** Conformal factor  $\psi$  in the  $xy$ -plane for a binary with rest masses  $m_{01} = 0.14$  and  $m_{02} = 0.06$ .

from [37, 25, 38, 39]) for point particles (dotted line) for small  $\omega$ . At intermediate  $\omega$  our results differ from point particle results and instead agree with previous results obtained by Taniguchi et al. [21]. Note that, while the agreement in  $M_{ADM}$  does not look as good as for  $J_{ADM}$ , the values for  $M_{ADM}$  from both methods still agree to better than 0.05%. With our current code we can construct initial data only up to  $\omega \sim 0.07$ . Beyond that point, already the first iteration of our elliptic solver fails. We suspect that our initial guess of simply using two spherical TOV stars with  $B^i = 0$  is not good enough for close configurations, and that the solver would succeed if we provided a guess that is closer to the true solution. Notice that while Taniguchi et al. [21] can extend their sequence to higher  $\omega$  they also did not record a turning point in either curve for this configuration.

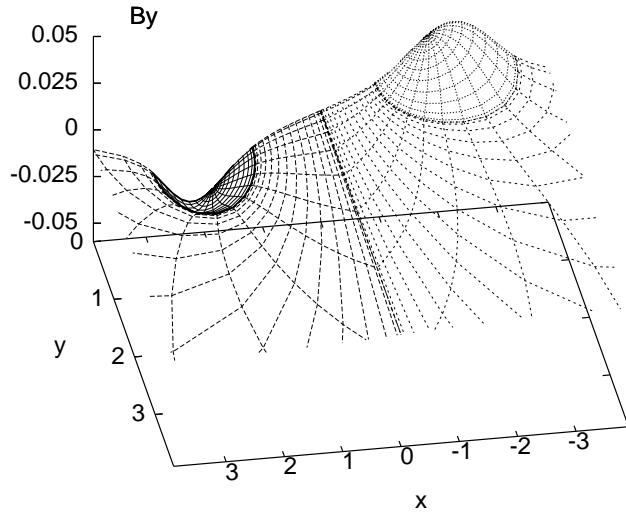


**Figure 6.** Largest shift component  $B_y$  in inertial coordinates for a binary with rest masses  $m_{01} = 0.14$  and  $m_{02} = 0.06$ .

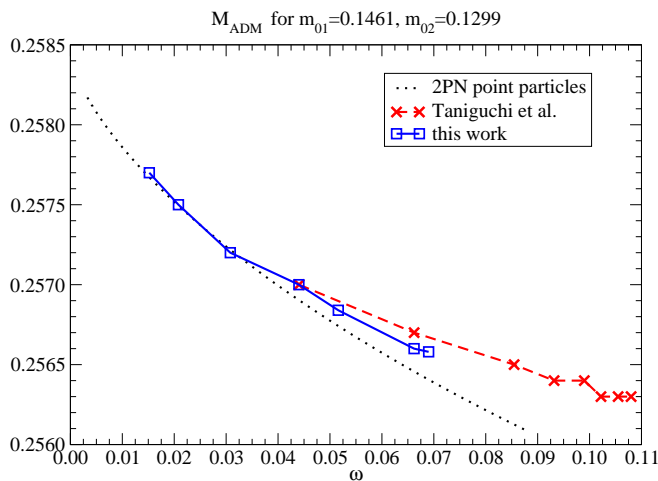


**Figure 7.** The ADM mass for a binary with rest masses  $m_{01} = 0.1461$  and  $m_{02} = 0.1299$  as a function of angular velocity in units of  $G = c = \kappa = 1$ . Shown are results for post-2-Newtonian point particles (dotted line), values from previous work [21] (crosses), and results from our new code (squares).

## 5. Discussion

The purpose of this paper is to introduce a new numerical method for the computation of binary neutron star initial data with the SGRID code [23]. The method uses six domains with different coordinate systems in each domain. The coordinates in four of these domains are closely related to the ones suggested in [30]. We have, however, added two extra domains with Cartesian coordinates to remove coordinate singularities. All our fields are  $C^\infty$  inside each domain. This allows us to use an efficient pseudo-spectral collocation method to solve the elliptic equations (12) associated with the initial data construction. Note that, we directly solve the 5 Eqs. (12), i.e. we do not split the

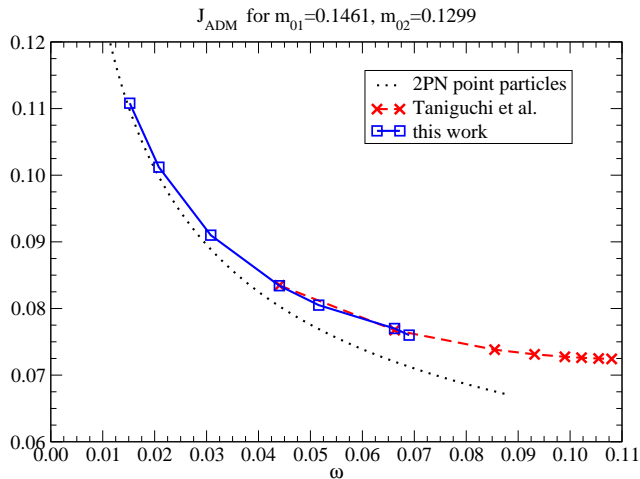


**Figure 8.** The ADM angular momentum for the same cases as in Fig. 7 in units of  $G = c = \kappa = 1$ .

shift in the momentum constraint into a vector and a gradient of a scalar, which would introduce an additional elliptic equation. Thus we have one less equation to solve than in the original Wilson-Mathews approach [9, 10]. Since two of our domains extend to spatial infinity we are able to easily impose the boundary conditions in Eq. (14) without the need of any approximations such as Robin boundary conditions.

At present we have only considered corotating configurations. The numerical method, however, could be easily extended to configurations with arbitrary spins, e.g. by following the approach in [20]. This approach involves the addition of one more elliptic equation for a velocity potential. The boundary conditions for this extra equation need to be imposed at the star surface, which is somewhat involved if one uses cubical domains as in [20]. With our new method, however, such boundary conditions can be easily imposed, since each star surface is a domain boundary.

It is well known that the star surfaces of close configurations can develop cusps due to tidal forces [19, 17, 20]. We have not investigated this issue with our new method yet, because our elliptic solver currently fails already during the first step for close configurations. We suspect that we need an initial guess that is better than two spherical TOV stars with vanishing shift  $B^i$ . We would like to point out, however, that our method should not have any additional problems with such cusps if they occur only along the  $x$ -axis (the line connecting the two stars). The reason is that the  $\sigma_{\pm}(B, \phi)$  which appear in the coordinate transformations and describe the star surfaces, can easily be chosen such that the domain boundaries have arbitrary cusps on the  $x$ -axis. Note that such cusp producing  $\sigma_{\pm}(B, \phi)$  are themselves perfectly smooth in  $A, B, \phi$  coordinates, so that we do not expect to lose spectral accuracy.

## Acknowledgments

It is a pleasure to thank Pedro Marronetti for useful discussions about NS initial data. This work was supported by NSF grant PHY-0652874.

- [1] B. Abbott et al. LIGO: The Laser Interferometer Gravitational-Wave Observatory. 2007. arXiv:0711.3041 [gr-qc].
- [2] <http://www.ligo.caltech.edu/>.
- [3] F. Acernese et al. The Virgo 3 km interferometer for gravitational wave detection. *J. Opt. A: Pure Appl. Opt.*, 10:064009, 2008.
- [4] VIRGO - <http://www.virgo.infn.it/>.
- [5] <http://geo600.aei.mpg.de/>.
- [6] B. Schutz. Gravitational wave astronomy. *Class. Quantum Grav.*, 16:A131–A156, 1999.
- [7] P. C. Peters and J. Mathews. Gravitational radiation from point masses in a Keplerian orbit. *Phys. Rev.*, 131:435–439, 1963.
- [8] P. C. Peters. Gravitational radiation and the motion of two point masses. *Phys. Rev.*, 136:B1224–B1232, 1964.
- [9] J. R. Wilson and G. J. Mathews. Instabilities in close neutron star binaries. *Phys. Rev. Lett.*, 75:4161, 1995.
- [10] J. R. Wilson, G. J. Mathews, and P. Marronetti. Relativistic Numerical Method for Close Neutron Star Binaries. *Phys. Rev.*, D54:1317–1331, 1996.
- [11] J. W. York. Conformal ‘thin-sandwich’ data for the initial-value problem of general relativity. *Phys. Rev. Lett.*, 82:1350–1353, 1999.
- [12] T. W. Baumgarte, G. B. Cook, M. A. Scheel, S. L. Shapiro, and S. A. Teukolsky. Binary Neutron Stars in General Relativity: Quasi-Equilibrium Models. *Phys. Rev. Lett.*, 79:1182–1185, 1997.
- [13] T. W. Baumgarte, G. B. Cook, M. A. Scheel, S. L. Shapiro, and S. A. Teukolsky. General Relativistic Models of Binary Neutron Stars in Quasiequilibrium. *Phys. Rev.*, D57:7299–7311, 1998.
- [14] G. J. Mathews, P. Marronetti, and J. R. Wilson. Relativistic Hydrodynamics in Close Binary Systems: Analysis of Neutron-Star Collapse. *Phys. Rev.*, D58:043003, 1998.
- [15] P. Marronetti, G. J. Mathews, and J. R. Wilson. Binary neutron star systems: From the Newtonian regime to the last stable orbit. *Phys. Rev.*, D58:107503, 1998.
- [16] Silvano Bonazzola, Eric Gourgoulhon, and Jean-Alain Marck. Numerical models of irrotational binary neutron stars in general relativity. *Phys. Rev. Lett.*, 82:892–895, 1999.
- [17] Eric Gourgoulhon, Philippe Grandclement, Keisuke Taniguchi, Jean-Alain Marck, and Silvano Bonazzola. Quasiequilibrium sequences of synchronized and irrotational binary neutron stars in general relativity. I. Method and tests. *Phys. Rev.*, D63:064029, 2001.
- [18] P. Marronetti, G. J. Mathews, and J. R. Wilson. Irrotational binary neutron stars in quasi-equilibrium. *Phys. Rev. D*, 60:087301, 1999.
- [19] Koji Uryu and Yoshiharu Eriguchi. A new numerical method for constructing quasi-equilibrium sequences of irrotational binary neutron stars in general relativity. *Phys. Rev.*, D61:124023, 2000.
- [20] Pedro Marronetti and Stuart L. Shapiro. Relativistic models for binary neutron stars with arbitrary spins. *Phys. Rev.*, D68:104024, 2003.
- [21] Keisuke Taniguchi and Eric Gourgoulhon. Quasiequilibrium sequences of synchronized and irrotational binary neutron stars in general relativity. III: Identical and different mass stars with  $\gamma = 2$ . *Phys. Rev.*, D66:104019, 2002.
- [22] Keisuke Taniguchi and Eric Gourgoulhon. Various features of quasiequilibrium sequences of binary neutron stars in general relativity. *Phys. Rev.*, D68:124025, 2003.
- [23] Wolfgang Tichy. Black hole evolution with the bssn system by pseudo-spectral methods. *Phys.*

- Rev.*, D74:084005, 2006.
- [24] C. W. Misner, K. S. Thorne, and J. A. Wheeler. *Gravitation*. W. H. Freeman, San Francisco, 1973.
  - [25] Wolfgang Tichy, Bernd Brügmann, Manuela Campanelli, and Peter Diener. Binary black hole initial data for numerical general relativity based on post-Newtonian data. *Phys. Rev. D*, 67:064008, 2003. gr-qc/0207011.
  - [26] Bernard J. Kelly, Wolfgang Tichy, Manuela Campanelli, and Bernard F. Whiting. Black hole puncture initial data with realistic gravitational wave content. *Phys. Rev.*, D76:024008, 2007.
  - [27] Alan P. Lightman, William H. Press, Richard H. Price, and Saul A. Teukolsky. *Problem Book in Relativity and Gravitation*. Princeton University Press, Princeton, NJ, 1975.
  - [28] Marcus Ansorg, Bernd Brügmann, and Wolfgang Tichy. A single-domain spectral method for black hole puncture data. *Phys. Rev. D*, 70:064011, 2004.
  - [29] Marcus Ansorg. A double-domain spectral method for black hole excision data. *Phys. Rev.*, D72:024018, 2005.
  - [30] Marcus Ansorg. Multi-Domain Spectral Method for Initial Data of Arbitrary Binaries in General Relativity. *Class. Quant. Grav.*, 24:S1–S14, 2007.
  - [31] Silvano Bonazzola, Eric Gourgoulhon, and Jean-Alain Marck. Numerical approach for high precision 3-D relativistic star models. *Phys. Rev.*, D58:104020, 1998.
  - [32] Timothy A. Davis and Iain S. Duff. An unsymmetric-pattern multifrontal method for sparse LU factorization. *SIAM J. Matrix Anal. Applic.*, 18(1):140–158, 1997.
  - [33] Timothy A. Davis and Iain S. Duff. A combined unifrontal/multifrontal method for unsymmetric sparse matrices. *ACM Trans. Math. Softw.*, 25(1):1–20, 1999.
  - [34] Timothy A. Davis. Algorithm 832: Umfpack v4.3—an unsymmetric-pattern multifrontal method. *ACM Trans. Math. Softw.*, 30(2):196–199, 2004.
  - [35] Timothy A. Davis. A column pre-ordering strategy for the unsymmetric-pattern multifrontal method. *ACM Trans. Math. Softw.*, 30(2):165–195, 2004.
  - [36] Timothy A. Davis. UMFPACK a sparse linear systems solver using the Unsymmetric MultiFrontal method:  
<http://www.cise.ufl.edu/research/sparse/umfpack/>.
  - [37] G. Schäfer and N. Wex. *Physics Lett. A*, 174:196, 1993.
  - [38] Wolfgang Tichy, Bernd Brügmann, and Pablo Laguna. Gauge conditions for binary black hole puncture data based on an approximate helical Killing vector. *Phys. Rev. D*, 68:064008, 2003.
  - [39] Wolfgang Tichy and Bernd Brügmann. Quasi-equilibrium binary black hole sequences for puncture data derived from helical killing vector conditions. *Phys. Rev. D*, 69:024006, 2004.